Electronic Coupling in a Highly Preorganized Bimetallic Complex Comprising Pyrazolate-Bridged $CpMn(CO)_2$ Moieties

Jens C. Röder,[b] Franc Meyer,*[a] Isabella Hyla-Kryspin,*[c] Rainer F. Winter,[d] and Elisabeth Kaifer[b]

Dedicated to Prof. Gottfried Huttner on the occasion of his 65th birthday

Abstract: By means of a multistep synthetic procedure a dimanganese complex has been prepared, in which a N,N′-bridging pyrazolate ligand spans two $CpMn(CO)_2$ subunits in a highly preorganized chelate arrangement. The X-ray crystallographic analyses of the Mn^IMn^I complex $K^+\mathbf{1}^-$ and of its non-chelate precursor complex elucidate details of the molecular structure, in particular an unusual pyrazolate binding mode in the solid state and intertwining of the CO ligands in the crowded bimetallic array $\mathbf{1}^-$. The Mn^IMn^I compound ($\mathbf{1}^-$), the mixed-valent Mn^IMn^{II} (**1**), and the oxidized $Mn^{II}Mn^{II}$ form ($\mathbf{1}^+$) have been characterized by various analytical and spectrosopic methods, such as electrochemistry, variable-temperature EPR spectroscopy, IR spectroelectrochemistry, and UV/Vis/NIR spectroelectrochemistry as well as by DFT and TD-DFT calculations. Strong electronic coupling in the mixed-valent complex is observed, but time- (and temperature-) dependent valence detrapping occurs, thus placing **1** in class II according to the Robin and Day assignment, close to the class II/III transition. From variable-temperature EPR spectroscopy a rough estimate of the activation energy and rate for thermal electron transfer can be deduced, with $E_{th}^{\ddagger} = 13.6\ kJ\,mol^{-1}$ and $k_{th} = 2.6 \times 10^{10}\ s^{-1}$ at 298 K. Unexpectedly, no intervalence CT transition for **1** is detected in solution, but one appears in the optical spectrum of solid **1**. The conclusions drawn from experiments are fully supported by DFT calculations that were carried out for all three forms of the dimanganese complex. A broken symmetry treatment for mixed-valent **1** reveals almost perfect localization of both spin and charge on one Mn center. According to TD-DFT the first excited states of **1** give rise to the IT processes in the NIR-energy region, as observed in the solid-state spectrum. The HOMOs are located at the Mn ions and are favorably arranged for π interactions with the bridging pyrazolate.

Keywords: density functional calculations · dinuclear complexes · electron transfer · manganese · mixed-valent compounds

Introduction

Cooperative phenomena between two or more proximate metal ions are attracting enormous attention in current chemical research. The major focus lies on the quest for cooperative reactivity,[1, 2] in particular for bimetallic reactivity patterns reminiscent of metalloenzyme activity, and on magnetic exchange interactions.[3] Also, there is continuing interest in understanding and tuning the electronic interaction between metal centers through or across bridging ligands, which is of fundamental relevance to, inter alia, electron transfer reactions in biology and electronic properties of materials.[4, 5] For the experimental study of electron transfer (ET) processes in mixed-valent dimetal compounds, systems with a formal low-spin d^5d^6 electronic configuration have received particular attention. The vast majority of such d^5d^6 mixed-valent complexes are based on ruthenium ammine fragments, since these exhibit favorable kinetic stability in both ruthenium +III and +II oxidation states.[6] A complementary organometallic species that fulfils the requirements of i) two neighboring oxidation states with d^5/d^6 electronic configuration in a useful potential region, ii) kinetic stability in these different oxidation states, and iii) the potential for efficient π backbonding with a bridging ligand, is the

[a] Prof. Dr. F. Meyer
Institut für Anorganische Chemie der Georg-August-Universität Göttingen
Tammannstrasse 4, 37077 Göttingen (Germany)
Fax: (0049)-551-393063
E-mail: franc.meyer@chemie.uni-goettingen.de

[b] Dr. J. C. Röder, Dr. E. Kaifer
Anorganisch-Chemisches Institut der Universität Heidelberg
Im Neuenheimer Feld 270, 69120 Heidelberg (Germany)

[c] Dr. I. Hyla-Kryspin
Organisch-Chemisches Institut der Universität Münster
Corrensstrasse 40, 48149 Münster (Germany)

[d] Dr. R. F. Winter
Institut für Anorganische Chemie der Universität Stuttgart
Pfaffenwaldring 55, 70569 Stuttgart (Germany)

Supporting information for this article is available on the WWW under http://www.wiley-vch.de/home/chemeurj.org/ or from the author.

DOI: 10.1002/chem.200204606

$CpMn(CO)_2$ fragment.[7, 8] This fragment has been extensively used as a stabilizing scaffold for unusual molecules[9] and as a redox center in mixed-valent compounds.[8, 10, 11, 12, 13] However, while the $CpMn(CO)_2$ fragment itself is very inert, $[CpMn(CO)_2L]$ complexes with classical 'inorganic' ligands L (e.g. first-row-element O and N donor ligands) exhibit notorious dissociative lability in their oxidized Mn^{II} forms, which has often hampered the isolation and detailed characterization of such species.[11]

We have recently reported a novel type of dinuclear $[\{CpMn(CO)_2\}_2L]$ array, where L is a N,N′-bridging pyrazolate that is covalently linked to the Cp spectator ligands at the manganese and spans the two Mn ions, thus giving a highly preorganized chelate arrangement in $\mathbf{1}^-$.[14] This system is closely related to the heavily studied type **A** complexes of cyclopentadienyl (Cp) ligands with functional amino or amido side chains,[15] since it can be described as a bimetallic version **B** in which the donor substituent tethered to the Cp moiety additionally serves a bridge function.[16] Such a strategy of formal coupling of two N-containing ligand compartments through a functionalized pyrazolate to constitute a highly preorganized dinuclear array has already been employed for mimicking cooperative effects in biomimetic coordination compounds.[17] Accordingly, type **B** systems are expected to give rise to cooperative phenomena in organometallic chemistry with the adjacent metal ions working in concert.

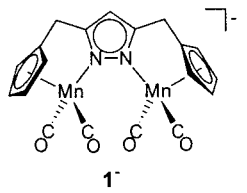

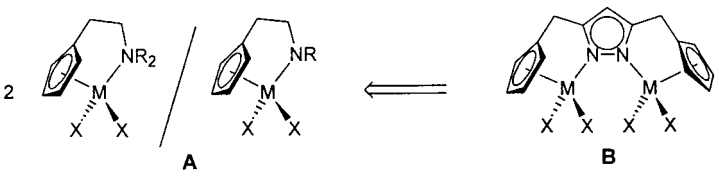

In the present context, the rigid chelate arrangement in $\mathbf{1}^-$ was anticipated to preclude dissociation of its $CpMn(CO)_2L$ moieties, thus allowing a detailed investigation by various analytical methods of the electronic structure of the dimanganese system in its different oxidation states. Some aspects of the structural and electronic properties of $\mathbf{1}^-$ have already been communicated.[14]

Results and Discussion

Synthesis and structural characterization: With the aim of preparing the sought-after ligand scaffolds for type **B** complexes, we initially treated the dichloro derivative of **2** with various Cp anion equivalents. However, while indenyl and fluorenyl side arms could readily be attached,[16] it proved difficult to introduce parent Cp by this route. $[CpMn(CO)_3]$ was thus employed as a 'protected' source of parent Cp. Still, in this case a palladium-catalyzed cross-coupling protocol[18] was required to achieve any reaction at all, and only monosubstitution was observed when starting from the dichloro derivative of **2** (Scheme 1).[19] Attachment of two $CpMn(CO)_3$ side arms to the pyrazole nucleus was finally accomplished by using the more reactive dibromo compound **2**,[20] in which the pyrazole-NH group is protected by a tetrahydropyranyl (thp) group. The procedure involves transmetalation of the lithiated $CpMn(CO)_3$ with $ZnCl_2$ and a subsequent $Pd(PPh_3)_2$-catalyzed cross-coupling reaction[18, 19] to form **3** in good yield according to Scheme 1. The product was purified by column chromatography, and the thp protecting group was then conveniently removed by treatment with acid to give **4**.

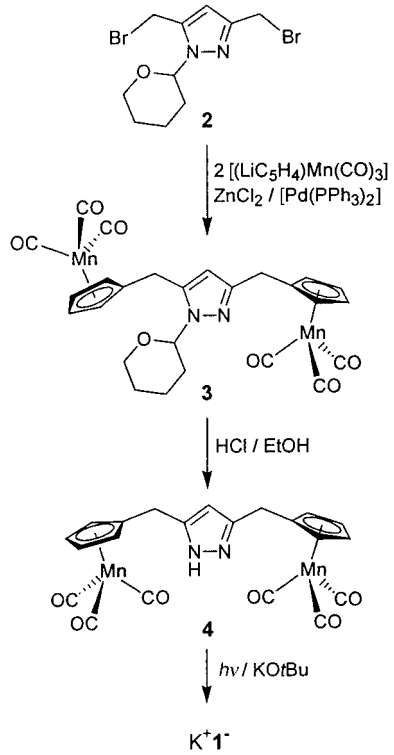

Scheme 1. Synthesis of $K^+\mathbf{1}^-$.

Compound **4** can be obtained as yellowish crystals from a CH_2Cl_2/light petroleum solution, and a single-crystal structure analysis was performed. The molecular structure of **4** is depicted in Figure 1, along with selected interatomic distances and bond angles. It confirms that **4** contains a protonated (noncoordinating) pyrazole group with two pendant $CpMn(CO)_3$ moieties. While the latter are still directed away from the pyrazole-N group in **4**, simple rotation around the spacer C–C bonds would bring the metal carbonyl fragments in a suitable arrangement to potentially interact with the pyrazole-N atoms. It should be noted that two different polymorphs of **4** could be crystallized from the CH_2Cl_2/light petroleum solution, which differ by the relative position of the pyrazole and $CpMn(CO)_3$ moieties due to distinct hydrogen-bonding patterns. In both cases, however, two pyrazole groups are arranged as dimers through $N\cdots H\cdots N$ interactions. Characteristic features of the different polymorphs will be analyzed in more detail elsewhere.[21]

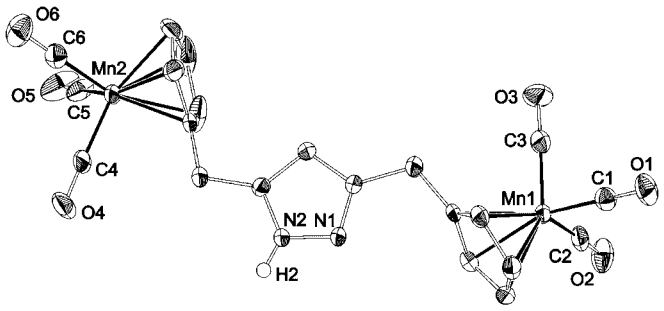

Figure 1. Molecular structure of **4** (40% probability ellipsoids). Selected interatomic distances [Å] and range of selected bond angles [°]: N1–N2 1.360(3), Mn1–C1 1.789(3), Mn1–C2 1.796(2), Mn1–C3 1.790(2), Mn2–C4 1.779(3), Mn2–C5 1.790(3), Mn2–C6 1.782(2), C1–O1 1.156(3), C2–O2 1.146(3), C3–O3 1.146(3), C4–O4 1.150(3), C5–O5 1.148(3), C6–O6 1.152(3); $C_{C\equiv O}$-Mn-$C_{C\equiv O}$ 90.5(2)–93.9(2).

For the preparation of mononuclear type **A** complexes in which MX_2 equals $Mn(CO)_2$, it has been reported that ring closure upon CO dissociation is very rapid if a favorable conformation brings the pendant side chain donor in close proximity to the metal center.[22] Extrusion of CO ligands by irradiation of **4** in THF and subsequent deprotonation using KO*t*Bu gave the first example of a type **B** bimetallic complex, $K^+\mathbf{1}^-$, as evidenced by the characteristic changes of the CO stretching frequencies (see below). Single crystals of $K^+\mathbf{1}^- \cdot 0.9$ THF obtained from THF/light petroleum were analyzed by X-ray crystallography. As discussed previously,[14] the crystals contain four independent (but similar) dimanganese(I) units of the anticipated constitution per asymmetric unit—one of them is depicted in Figure 2.

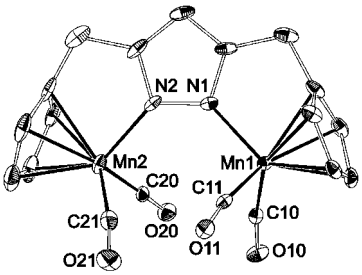

Figure 2. Molecular structure of $\mathbf{1}^-$ (30% probability ellipsoids). Selected interatomic distances [Å] and range of selected bond angles and dihedral angles [°]; values for the other three independent molecules in square brackets: Mn1–N1 2.034(4) [2.032(4), 2.066(3), 2.047(4)], Mn2–N2 2.053(4) [2.060(4), 2.053(4), 2.033(4)], Mn–$C_{C\equiv O}$ 1.748(5)–1.791(6) [1.747(5)–1.772(5), 1.746(5)–1.780(5), 1.748(5)–1.766(5)], $C_{C\equiv O}$–O 1.149(6)–1.177(6) [1.166(5)–1.174(5), 1.164(5)–1.177(5), 1.174(5)–1.175(5)]; $C_{C\equiv O}$-Mn-N 98.6(2)–102.9(2) [100.0(2)–103.8(2), 102.3(2)–104.7(2), 96.3(2)–102.8(2)], Mn1-N1-N2-Mn2 27.9(1) [22.3(1), 10.3(1), 34.3(1)].

In accordance with expectations, upon going from **4** to $\mathbf{1}^-$ the mean value for Mn–$C_{C\equiv O}$ decreases (1.788 Å in **4** versus 1.761 Å in $\mathbf{1}^-$), while the mean C–O bond length of the carbonyl ligands increases (1.150 Å in **4** versus 1.170 Å in $\mathbf{1}^-$). This expresses the larger extent of Mn → CO π-backbonding in the $CpMn(CO)_2L$ moiety upon replacement of a third CO ligand by the pyrazolate group.

Several other features of the solid-state structure of $K^+\mathbf{1}^- \cdot 0.9$ THF are worth mentioning: i) The dimanganese entities are connected through the potassium countercations to form a three-dimensional coordination polymer in which the K^+ ion exhibits unusual η^5 π interactions with the pyrazolate heterocycle. η^5 coordination to a pyrazolate group is rare and has only been reported in a few cases,[23] while the $\eta^1{:}\eta^1{:}\eta^5$ binding mode observed in $K^+\mathbf{4}^-$ is unprecedented.[24] ii) The coordination sphere of two of the four crystallographically distinct K^+ ions is completed by three O atoms of Mn-bound CO and by one THF solvent molecule, while the other two K^+ ions are O-coordinated by four CO ligands. Those latter K^+ ions display a remarkably short additional side-on π interaction with one CO ligand that is already end-on bound to a second K^+ ion. According to a CSD[26] search these are among the shortest side-on $K^+ \cdots CO$ contacts detected thus far.[25]

In the present context, some molecular features of $\mathbf{4}^-$ deserve particular attention: the angles N-Mn-$C_{C\equiv O}$ are rather large (mean value 101.9°) compared to other $[CpMn(CO)_2L]$ complexes (L = N donor ligand; 92.6–98.1° according to a CSD search) and the CH_2 spacer groups that link the Cp and the pyrazolate groups are bent by about 10° out of the Cp plane toward the Mn ions, indicating a somewhat strained chelate situation. In addition, both metal ions are displaced out of the plane of the pyrazolate heterocycle, while at the same time the two $Mn(CO)_2$ moieties are slightly twisted with respect to each other. This appears to result from steric congestion within the bimetallic pocket and concomitant intertwining of the CO ligands according to the situation in **I**. Similarly, steric hindrance between the Mn-bound CO ligands and a Zn-bound Cl atom has been considered to explain structural features of the related heterobimetallic MnZn complex **5**.[19] Finally, the π plane of the bridging pyrazolate in $\mathbf{1}^-$ roughly coincides with the mirror plane of the $Mn^{II}(CO)_2$ fragments, which is a favourable situation for stabilizing electronic π interactions.[7, 8]

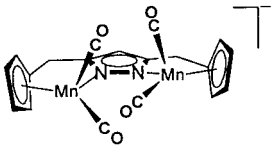

I

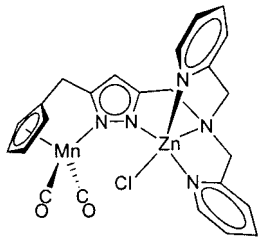

5

Discussion of electrochemical and spectroscopic results: The Mn^IMn^I compound $\mathbf{1}^-$ is easily oxidized, for example by air. Its cyclic voltammogram in THF reveals two well-separated reversible redox waves at $E_{1/2} = -0.37$ V and $E_{1/2} = +0.14$ V (Figure 3),[27] corresponding to the formation of the Mn^IMn^{II} (d^5/d^6) and the fully oxidized $Mn^{II}Mn^{II}$ (d^5/d^5) species. The rather large separation of these single-electron processes ($\Delta E_{1/2} = 509$ mV) suggests strong electronic coupling and significant stabilization of the mixed-valent compound **1**,

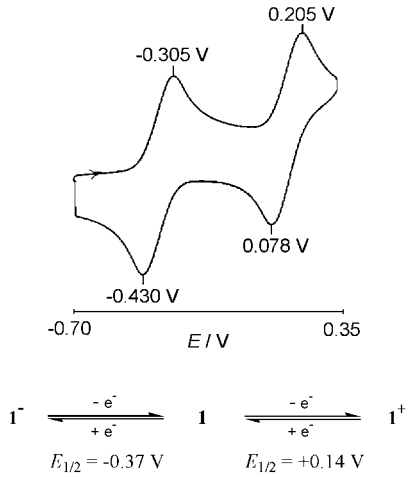

Figure 3. Cyclic voltammogram of $\mathbf{1}^-$ recorded on a platinum electrode in THF containing 0.1M $N(n)Bu_4^+PF_6^-$; scan speed 200 mV s^{-1}.[27]

and a comproportionation constant $K_{comp} = 4.1 \times 10^8$ for the equilibrium given in Equation (1) can be calculated by using the expression in Equation (2).[28]

$$\mathbf{1}^- + \mathbf{1}^+ \overset{K_{comp}}{\rightleftharpoons} 2\mathbf{1} \quad (1)$$

$$\Delta E_{1/2} = (RT/nF)\ln(K_{comp}) \quad (2)$$

Compound **1** can be prepared on a preparative scale by oxidation of $\mathbf{1}^-$ with $AgBF_4$ and was isolated as a red powder. It is a rare example of a neutral d^5/d^6 mixed-valent complex, which is of particular interest because the absence of charge trapping in nonpolar solvents is expected to favor a high degree of delocalization. To gain insight into the electronic structure of mixed-valent **1**, a detailed investigation by EPR, UV/vis/NIR, and IR spectroscopy was performed.

The EPR spectrum of **1** in 2-methyltetrahydrofuran at 293 K shows an 11-line pattern ($g_{iso} = 2.029$; $a(^{55}Mn)_{iso} = 2.83$ mT; Figure 4), confirming equivalence of the two metal centers on the EPR time scale. A spectrum in frozen solution (123 K), however, indicates localized valency, since the spectrum is typical for $[CpMn^{II}(CO)_2L]$ compounds with approximate axial symmetry of the g tensor, that is with anisotropic hyperfine coupling to a single ^{55}Mn nucleus.[29] To locate the conversion between EPR-localized and -delocalized states, variable-temperature EPR spectra were measured (Figure 4). Transition between the isotropic 11-line pattern and a 6-line profile occurs at about 185 K, where the solution (2-methyltetrahydrofuran/3-methylcyclopentane 1:4) is still fluid. If one assumes that sufficiently slow intramolecular electron transfer at low temperature is the reason for the 'coalescence phenomenon', a rough estimate of the activation energy $E_{th}^{\neq}$ and the thermal electron transfer rate k_{th} can be derived from Gagné's approximation [Eq. (3)],[30] giving $E_{th}^{\neq} = 13.6$ kJ mol^{-1} and $k_{th} = 2.6 \times 10^{10}$ s^{-1} at 298 K.

$$k_{th} = (kT/h)e(-E_{th}^{\neq}/RT) \quad (3)$$

Further oxidation does not proceed readily when using $AgBF_4$ as the oxidant, but is achieved by stirring a solution of $\mathbf{1}^-$ in THF under an atmosphere of oxygen for 1 h. IR

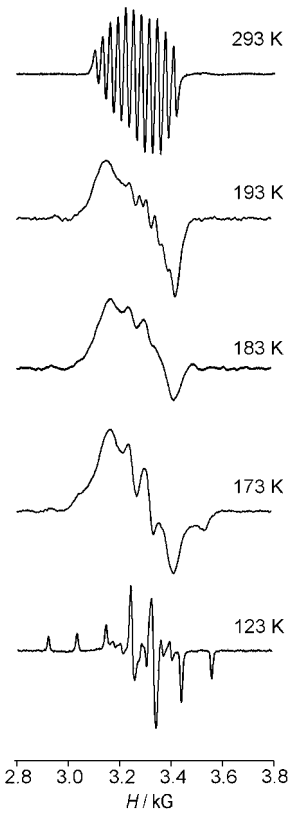

Figure 4. EPR spectra of the mixed-valent complex **1** in 2-methyltetrahydrofuran/3-methylcyclopentane (1:4) at selected temperatures.

spectroscopy confirms that the $CpMn(CO)_2$ fragments are still intact in the oxidized product, although the anticipated product $\mathbf{1}^+$ could not be isolated in pure form. A solution EPR spectrum at 198 K reveals a sextet of lines with g_{iso} centered around 2.023 and an isotropic coupling constant $a(^{55}Mn)_{iso} = 5.82$ mT (Figure 5). The latter value is roughly twice as large as the coupling observed for the mixed-valent species **1**, in

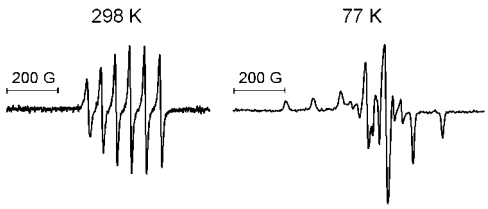

Figure 5. EPR spectra of the dimanganese(II) complex $\mathbf{1}^+$ in 2-methyltetrahyrofuran at 298 K and 77 K.

accordance with expectations. The EPR spectrum of the fully oxidized isovalent species $\mathbf{1}^+$ in frozen solution is very similar to the low-temperature spectrum of **1**. It should be emphasized though, that a pyrazolate-bridged structure (i.e. a constitution similar to that of $\mathbf{1}^-$) is not proven for the O_2-oxidized product, and the absence of any dipolar coupling which might be expected for the EPR spectra of two closely spaced Mn^{II} ($S = ½$) ions is to be noted.[31]

Neither for **1** nor for $\mathbf{1}^+$ coupling to the pyrazole nitrogen atoms is detected by EPR spectroscopy which points to the SOMO being localized on the $CpMn(CO)_2$ moieties with at

best little contribution of the bridging ligand, in accordance with the electronic structure calculations described below.

To gain further information on the electronic structure of the individual species, stepwise oxidation of $\mathbf{1}^-$ in dichloroethane was monitored by IR and UV/Vis/NIR spectroscopy in an OTTLE cell. Figure 6 displays the changes of the IR bands

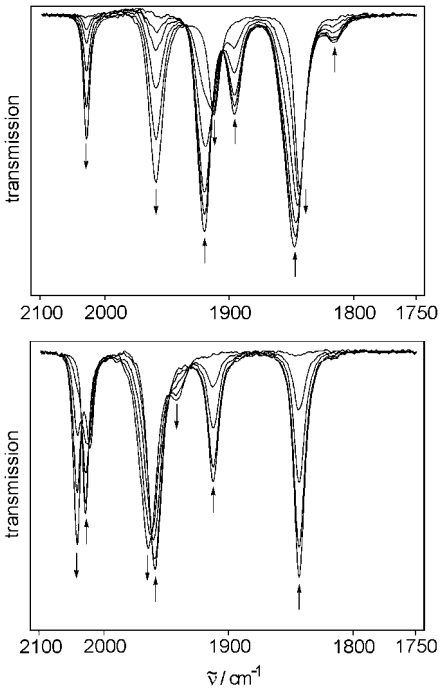

Figure 6. IR spectroscopic changes during gradual oxidation $\mathbf{1}^- \rightarrow \mathbf{1}$ (top) and $\mathbf{1} \rightarrow \mathbf{1}^+$ (bottom) in an OTTLE cell.

in the CO stretching region that occur upon gradual electrolysis of $\mathbf{1}^-$ to form **1** (upper), and upon continued electrolysis to give the doubly oxidized product $\mathbf{1}^+$ (lower). The presence of several isosbestic points confirms clean conversion between the different species. Furthermore, these processes are fully reversible since the spectrum of the starting material is restored upon re-reduction. The resulting IR spectra of $\mathbf{1}^-$, **1**, and $\mathbf{1}^+$ are compared in Figure 7, together with the spectra of their precursor complexes.

The prominent pair of CO stretching bands characteristic for the $CpMn(CO)_3$ fragments in **4** (2015 and 1927 cm^{-1}; Figure 7a)[32] is shifted to lower energy upon irradiation (1916 and 1843 cm^{-1}; Figure 7 b), indicating the anticipated loss of CO. Subsequent addition of KO*t*Bu to form $K^+\mathbf{1}^-$ causes these resulting bands to change only slightly, but two additional small features are now discernible (this is discussed in more detail below). The overall band pattern of the CO stretches for $\mathbf{1}^-$ (Figure 7c) is retained after full oxidation to give $\mathbf{1}^+$, but all bands are shifted to higher energy by around 120 cm^{-1} (Figure 7e), in accordance with expectations for a full unit increase in metal oxidation state.[33] These findings are consistent with the presence of two equivalent Mn^I centers in **4** and $\mathbf{1}^-$, and two equivalent Mn^{II} centers in the cation $\mathbf{1}^+$. In contrast, four strong CO absorptions are observed for the neutral mixed-valent Mn^IMn^{II} compound **1** (2028, 1958, 1912,

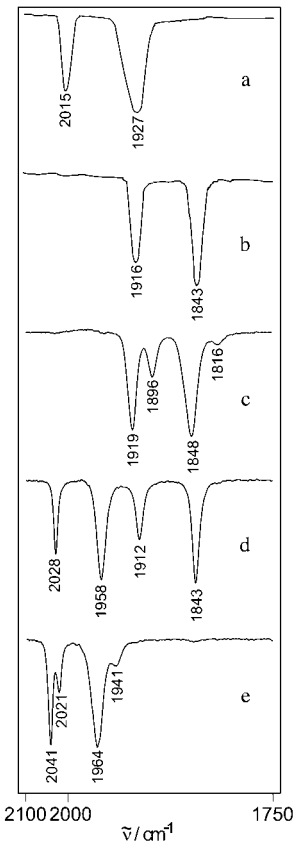

Figure 7. IR spectra in the CO stretching region for complex **4** before (a) and after (b) irradiation in THF, following addition of KO*t*Bu to give $\mathbf{1}^-$ (c) and upon gradual oxidation to **1** (d) and $\mathbf{1}^+$ (e).

and 1843 cm^{-1}), thus confirming that **1** is a valence-trapped species on the short vibrational time scale ($\sim 10^{-13}$ – 10^{-14} s).[34]

Some comment should be made on the two low-intensity bands discernible in the spectra of both $\mathbf{1}^-$ and $\mathbf{1}^+$. Several control experiments established unambiguously that these features do not arise from impurities. This is further supported by the clean isosbestic points observed in Figure 6a and b, where the small bands and the more intense main bands rise and decrease simultaneously during the spectroelectrochemical experiment. Also, the IR spectrum of powdered single crystals of $K^+\mathbf{1}^-$ in KBr gives an identical band pattern. Interestingly, similar small features have previously been observed for some other complexes bearing two $CpMn(CO)_2L$ groups in close proximity.[12] These additional bands are assumed to result from vibrational coupling of the adjacent metal dicarbonyl fragments. In the case of $\mathbf{1}^-$ and $\mathbf{1}^+$, intertwining of the CO ligands within the bimetallic pocket (compare **I**) leads to an apparent C_2 symmetry of the bimetallic scaffold, which should give rise to each two IR-active CO stretching vibrations of the *A* and *B* representations.

Evidently, in $\mathbf{1}^-$ and $\mathbf{1}^+$ the CO stretches of the two metal dicarbonyl fragments cannot be regarded as vibrationally independent. This interpretation is fully supported by the DFT calculations described below. It is also corroborated by considering the IR spectrum of the irradiated starting material **4** (Figure 7b): prior to addition of KO*t*Bu, the

pyrazole heterocycle is still protonated and cannot function as a bridging moiety. The spectrum depicted in Figure 7b is thus assigned to either a species with two dangling $CpMn(CO)_2(THF)$ moieties or to a species with only one of the $CpMn(CO)_2$ fragments already bound to the single accessible N atom of the pyrazole (with the two expected sets of IR bands accidentally coinciding in the latter case; note that only a minor shift occurs upon coordination of the second pyrazole-N atom). It is not until the addition of KO*t*Bu that the bridging mode of the pyrazolate is induced, which forces the two $CpMn(CO)_2$ fragments into close proximity and thereby causes vibrational coupling of their CO stretches (Figure 7c).

The results obtained for $\mathbf{1}^{-/0/+}$ can be compared to the experimental findings for the related complex **5**,[19] which features only a single $CpMn(CO)_2$ moiety linked to a second redox-inactive zinc ion through a pyrazolate bridge. Complex **5** gives a good estimate of the redox properties and spectroscopic characteristics of an electronically isolated $CpMn(CO)_2$ unit in that particular coordination environment. It displays a single reversible oxidation at -0.20 V versus SCE in CH_2Cl_2,[19] that is intermediate between the two sequential oxidation potentials observed for $\mathbf{1}^-$.[35] The CO stretches of **5** are found at 1910 and 1835 cm^{-1} in dichloroethane, while those for its oxidized Mn^{II} form appear at 2041 and 1964 cm^{-1}. Both data pairs are in good agreement with the values obtained for $\mathbf{1}^-$ and $\mathbf{1}^+$, respectively.

Vibrational coupling of the CO stretches for $\mathbf{1}^-$ and $\mathbf{1}^+$ and the resulting IR spectrum of higher order hampers any more detailed analysis of the spectral shifts for deducing a quantitative estimate of the charge distribution between the two metal centers in the mixed-valent complex **1**.[13, 36] However, from Figure 7 it is clear that the higher and lower energy pair of bands for **1**, which are assigned to the valence-trapped Mn^{II} and Mn^{I} sites, are barely shifted from the energies for the fully oxidized $Mn^{II}Mn^{II}$ ($\mathbf{1}^+$) and the fully reduced $Mn^{I}Mn^{I}$ ($\mathbf{1}^-$) forms, respectively. Since carbonyl shifts are considered to track the charges on the metal ions, these experimental findings point to a pronounced charge localization in the mixed-valent compound **1**.

Taken together, the EPR- and IR-spectroscopic results place **1** into class II of mixed-valent compounds according to the assignment by Robin and Day. The phenomenon of time- (and temperature-)dependent valence detrapping as observed in EPR spectroscopy indicates its proximity to the class II/III transition,[37] while the large $\Delta E_{1/2}$ value is more characteristic of a genuine class III species.[38]

UV/Vis/NIR spectroelectrochemistry in dichloroethane is shown in Figure 8 for the $\mathbf{1}^- \rightarrow \mathbf{1}$ (top) and the $\mathbf{1} \rightarrow \mathbf{1}^+$ conversions (bottom). Again, both processes are fully reversible. The absorption at 400 nm for $\mathbf{1}^-$ is assigned to a $Mn^{I} \rightarrow \pi^*$(pyrazolate) MLCT transition,[39] whereas the band at 468 nm that develops concomitant with oxidation to **1** is attributed to the π(pyrazolate) $\rightarrow Mn^{II}$ LMCT transition. These assignments are in full accordance with the results of time-dependent DFT calculations (vide infra). As expected, the latter band increases in intensity upon oxidation of the second metal due to the presence of two chromophores, but shifts to higher energy (400 nm). Contrary to expectation,

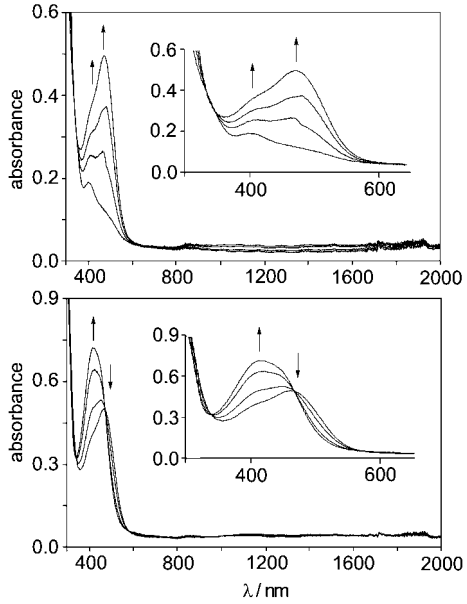

Figure 8. UV/Vis/NIR spectroscopic changes during gradual oxidation $\mathbf{1}^- \rightarrow \mathbf{1}$ (top) and $\mathbf{1} \rightarrow \mathbf{1}^+$ (bottom) in dichloroethane in an OTTLE cell.

however, no intense long-wavelength intervalence transition (IT) is detectable in the optical spectrum of **1** in dichoroethane or THF measured to wavelengths as high as 3000 nm. It has been reported that IT transitions can be very weak in some cases,[40] but interestingly the optical spectrum of **1** in the solid state (diffuse reflectance) shows an intense double-humped band in the near-IR range which is absent in the optical reflectance spectrum of the reduced dimanganese(I) complex $K^+\mathbf{1}^-$ (Figure 9). While the physical state of a sample

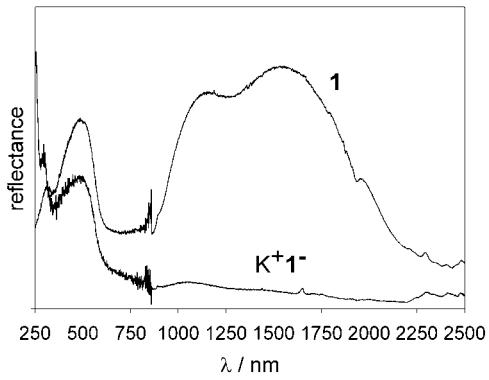

Figure 9. Optical spectra of solid $K^+\mathbf{1}^-$ and **1** (diffuse reflectance).

can influence the electron transfer rate, for example by coupling the electronic structure to the lattice or trapping of an asymmetry in the solid state,[41] it is temptimg to assign this NIR absorption of solid **1** to an IT transition. It is important to mention, however, that broad low-energy (near- to mid-IR) electronic absorptions which are ligand-field in origin have been detected for 17-electron $[CpMn(CO)_2L]$ complexes.[42] These absorptions arise from the splitting of the degenerate e-type orbital pair (in C_{3v}-symmetric $[CpMn(CO)_3]$; resulting from the putative t_{2g} set) into a′ and a″ orbitals due to symmetry lowering in C_s-symmetric $[CpMn(CO)_2L]$. While

the possible presence of such d-d transitions in the energy range where the IT bands are expected and where the near-IR bands are observed for solid **1** introduces some ambiguity into any band assignments, we note that the high intensity of these two bands argues against a (dominant) contribution of d – d transitions.

Spectral deconvolution of the overlapping NIR features of solid **1** by modeling the band envelope with two Gaussian curves gives $\tilde{\nu}_{max}(1) = 8703\ cm^{-1}$ ($\Delta\tilde{\nu}_{1/2} = 3440\ cm^{-1}$) and $\tilde{\nu}_{max}(2) = 6083\ cm^{-1}$ ($\Delta\tilde{\nu}_{1/2} = 1760\ cm^{-1}$) (see Figure S1 in the Supporting Information). A commonly used criterion for analyzing mixed-valency in solution is a comparison of the experimental bandwidth ($\Delta\tilde{\nu}_{1/2}$) with that predicted by Hush for class II systems according to $\Delta\tilde{\nu}_{1/2}(calcd) = (2310\ \tilde{\nu}_{max})^{1/2}\ cm^{-1}$. Experimental bandwidths less than the predicted ones are usually considered diagnostic for intrinsically delocalized class III systems. When the above relation is applied to the reflectance band of solid **1** at 8703 cm^{-1}, the experimental bandwidth (3440 cm^{-1}) is considerably narrower than calculated (4480 cm^{-1}), and this is even more valid for the band peaking at 6083 cm^{-1}. IT transition energies for class II mixed-valent systems are known to be quite sensitive to molecular environment,[41] and the appearance of multiple intervalence transitions has been reported for several cases.[43] Those findings have been interpreted in terms of multiple ground state or excited state forms due to, inter alia, large spin-orbit coupling effects (which are not expected in the present case) or symmetry reduction that arises from selective solvation or ion pairing. If one assumes that the NIR bands in the reflectance spectrum of **1** originate from IT transitions (which is corroborated by TD-DFT calculations, vide infra), an environmental effect also seems most plausible for the double-humped band shape in the present case. It should be noted though, that the optical transitions at 6083 and 8703 cm^{-1} correspond to energies $E_{op} \approx 73$ and 104 $kJ\,mol^{-1}$, respectively. This is considerably higher than expected for a Robin and Day class II system, since the relation $E_{op} = 4E_{th} - H_{AB}$ (H_{AB} is the electronic coupling) predicts a value well below 55 $kJ\,mol^{-1}$ in the case of $E_{th} = 13.6\ kJ\,mol^{-1}$ (as deduced from the EPR spectra, vide supra). Again, discrepances may be attributed to the different physical state, that is solution versus solid state.

At present, we have no conclusive explanation for the absence of IT absorptions for **1** in solution, but a scenario should be discussed which takes into account the notorious lability of (low-spin d^5) $[CpMn^{II}(CO)_2L]^+$ species. It assumes that the pyrazolate-bridged species **1** is only present as a minor component in equilibrium with the solvent-stabilized open form **1′** (Scheme 2). Spectroscopic methods that are fast with respect to the rate of the chemical equilibrium would solely detect the dominant species **1′**, for example four carbonyl IR bands (where the Mn^I site receives full negative charge of the pyrazolate) and the absence of any optical IT absorption. Methods with a time scale slower than the chemical process should reveal the signature of a strongly coupled (delocalized) system due to very fast electron transfer via the minor species **1**. According to this situation, fast intramolecular electron transfer in **1** would be gated by the rate of intramolecular dissociation of the hemilabile pyrazolate bridge (i.e. by the rate of an intramolecular chemical preequilibrium process), which could be of the order of the EPR time scale. Second-order rate constants in the order of $10^4\ M^{-1}s^{-1}$ have been determined for the ligand exchange reaction in Equation (4),[44] and such reactions might still be much faster in the case of ring closure and ring opening by a pendant chelate arm.[22] However, we consider this scenario unlikely due to the following reasons: i) addition of pyridine to the dichloroethane or thf solution in the spectroelectrochemical experiments did not lead to any noticable changes in the CO stretching vibrations of **1** (and $\mathbf{1}^+$), as would be expected for pyridine coordination to the dangling $CpMn^{II}(CO)_2$ fragment in **1′**, and ii) the solution IR spectrum of the dimanganese(II) species $\mathbf{1}^+$ (Figure 6 and Figure 7) exhibits the typical pattern which we assume to arise from the intertwining of the CO ligands according to the situation depicted in **I**, indicating integrity of the pyrazolate-bridged bimetallic arrangement upon oxidation to the Mn^{II} state.

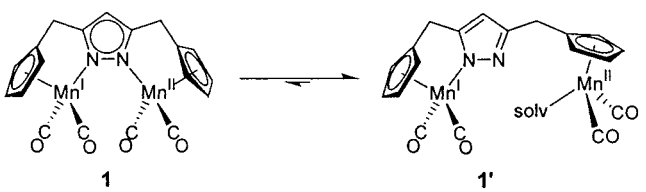

1 1′

Scheme 2. Possible equilibrium between the chelate form **1** and the solvent-stabilized open form **1′**, which is assumed to not be of any relevance.

$$[CpMn(CO)_2L] + L' \rightarrow [CpMn(CO)_2L'] + L \quad (4)$$

Theoretical Investigations: To describe the electronic structures of the complexes $\mathbf{1}^{-/0/+}$ and to gain deeper insight into the extent of spin and charge delocalization in the mixed-valence form **1**, we have carried out DFT calculations on the C_2-symmetric singlet, doublet, and triplet electronic states of $\mathbf{1}^-$, **1**, and $\mathbf{1}^+$, respectively, and we have performed a broken-symmetry treatment for the mixed-valent complex **1**. We started our investigations with geometry optimizations in the C_2 symmetry point group for the ground-state molecular structures $^1A(\mathbf{1}^-;C_2)$, $^2A(\mathbf{1};C_2)$, and $^3B(\mathbf{1}^+;C_2)$. These calculations were followed by geometry optimizations without any symmetry constraints for the doublet state of **1**, $^2\mathbf{1}(C_1)$. Some selected optimized parameters are collected in Table 1. According to the vibrational analyses there are no imaginary modes, and consequently all optimized structures represent minima on the potential energy surfaces.

The DFT-optimized parameters corresponding to the gas-phase structure of $\mathbf{1}^-$ are in good agreement with the values determined experimentally for solid $K^+\mathbf{1}^-$ (Table 1), and hence we assume the DFT metric parameters for the oxidized species also represent well the structural characteristics of the Mn^IMn^{II} and $Mn^{II}Mn^{II}$ complexes. Since it was not possible to characterize **1** and $\mathbf{1}^+$ by X-ray measurements, a closer comparison of the data from Table 1 is instructive for an understanding of the oxidized species. For the C_2-symmetric species, an increase of the $Mn{-}C_{C\equiv O}$ and a decrease of the C–O bond lengths is discernible upon going from $\mathbf{1}^-$ to **1** and further to $\mathbf{1}^+$. These changes are consistent with the lower

Table 1. Selected metric parameters of $\mathbf{1}^-$, $\mathbf{1}$, and $\mathbf{1}^+$; experimental values (for $K^+\mathbf{1}^-$) and DFT optimized values in C_2 symmetry point group for the singlet (^{1}A), doublet (^{2}A) and triplet (^{3}B) ground states, respectively, and for the doublet state of **1** without symmetry constraints, $^2\mathbf{1}(C_1)$. Distances are given in Å, angles in degrees.

	exp ($K^+\mathbf{1}^-$)[a]	^{1}A($\mathbf{1}^-;C_2$)	^{2}A($\mathbf{1};C_2$)	$^2\mathbf{1}(C_1)$[b]	^{3}B($\mathbf{1}^+;C_2$)
Mn–N	2.047	2.078	2.023	2.078(1.957)	1.993
Mn–$C_{C\equiv O}$(1)	1.770	1.782	1.812	1.775(1.854)	1.856
Mn–$C_{C\equiv O}$(2)	1.751	1.780	1.808	1.783(1.851)	1.849
Mn–$C(Cp)_{av}$	2.136	2.173	2.168	1.937(2.174)	2.169
$C_{C\equiv O}$–O(1)	1.174	1.160	1.149	1.160(1.138)	1.137
$C_{C\equiv O}$–O(2)	1.166	1.159	1.149	1.158(1.139)	1.139
N1–N2	1.380	1.362	1.353	1.369	1.378
∢ $C_{C\equiv O}$(1)-Mn-N	100.5	96.2	96.8	95.6(96.3)	96.4
∢ $C_{C\equiv O}$(2)-Mn-N	103.3	101.6	102.9	102.2(103.2)	103.6
∢ Mn-N1-N2	133.8	134.4	134.4	134.1(133.7)	134.9
∢ Mn1-N1-N2-Mn2	23.7	24.4	26.1	29.7	33.7

[a] Average values. [b] The first values refer to the Mn1 part and values in parentheses refer to the Mn2-part of **1**.

extent of π-backbonding in the oxidized compounds and explain the observed shifts of the CO stretching vibrations. The distances Mn–C(Cp) and the bond angles N-Mn-$C_{C\equiv O}$ and N-N-Mn are not influenced significantly by oxidation. However, the dihedral angle Mn-N-N-Mn becomes slightly larger in the oxidized forms. In the case of $^2\mathbf{1}(C_1)$ the Mn1 part of the molecule shows almost the same geometric features as the Mn^I ions in the singlet state ^{1}A of $\mathbf{1}^-$, whereas the Mn2 part adopts those of the Mn^{II} ions in the triplet state ^{3}B of $\mathbf{1}^+$ (Table 1).

According to the DFT wave function, the six highest occupied MOs of $\mathbf{1}^-$ are symmetry-adapted linear combinations of atomic orbitals with predominant Mn1 and Mn2 3d character ([Eq. (5)] with $i = x^2 - y^2, z^2, xy$).

$$\Psi_+ = N_+(3d_{i1} + 3d_{i2}) \text{ and } \Psi_- = N_-(3d_{i1} - 3d_{i2}) \quad (5)$$

The same combinations are found in the wave functions of the C_2-symmetric oxidized forms. As an example the HOMO(3a) and HOMO-1(3b) of $\mathbf{1}^-$ together with their occupations in the particular states are shown in Figure 10. It is apparent that both MOs have antibonding admixtures from the π-pyrazolate system.

Removal of an electron from the ^{1}A ground state of the Mn^IMn^I compound $\mathbf{1}^-$ requires 57.02 kcal mol^{-1}, but removal of a second electron from the ^{2}A ground state of the $Mn^{II}Mn^I$ complex **1** is much more demanding and requires 119.7 kcal mol^{-1} (Table 2). These values are in accord with the large separation of the two reversible one-electron redox waves in the cyclic voltammetry experiment (Figure 3), and they confirm the relative stabilization of the mixed-valent form **1** toward disproportionation. Furthermore, the ^{2}B(Ψ_+) electronic state of **1** is only 0.5 kcal mol^{-1} less stable than the ^{2}A(Ψ_-) ground state, suggesting that the release of symmetry constraints on the wave function may lead to a significant mixing and, as a result, to localized states [Eq. (6)].

$$\Psi = c_1\Psi_+ \pm c_2\Psi_- \quad (6)$$

There are many cases known in the literature, especially for deep core and metal electron ionizations, where the wave function of the lowest energy solution exhibits a lower symmetry than the full Hamiltonian.[36, 45]

Calculated charge and spin distributions in the investigated compounds are collected in Table 2. These data clearly show that upon removal of an electron from a Mn center, the electron density flows from the surrounding ligands toward the metals to compensate for the loss of electron density at the Mn centers. Such reorganization of electron density is well documented, especially in the

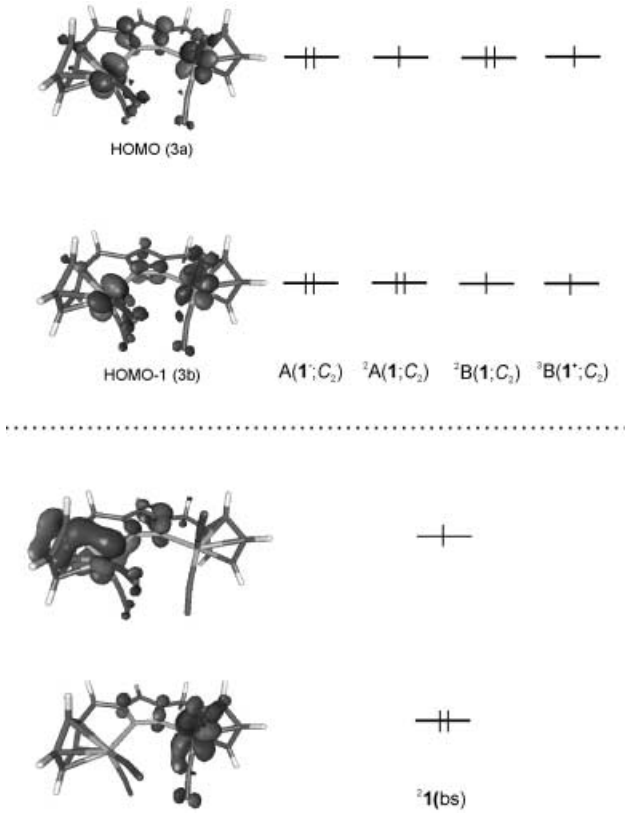

Figure 10. MO shapes and occupation patterns of the valence MOs derived from the B3LYP C_2-symmetric wave functions of $\mathbf{1}^{-/0/+}$ (top) and for the broken-symmetry solution of **1** (bottom).

case of electron-rich 3d transition metals.[36, 46] Naturally, in the case of symmetrical wave functions (C_2 symmetry) the charge and spin is equally distributed over symmetry equivalent sites. However, the broken symmetry solution for **1**, ^{2}**1**(bs), leads to a strongly localized ground state wave function (Figure 10 (bottom), Table 2). Contrary to the symmetric wave function, the open shell orbital from the broken symmetry solution displays bonding admixture of the pyrazolate π MO which in turn may facilitate the communication with the other half of the bimetallic molecule. The localization

Table 2. Relative energies (kcal mol^{-1}), $<S^2>$ values, atomic spin densities (ρ), and Mulliken charges (q) of the Mn atoms and ligands for the singlet, doublet, and triplet states of the complexes $\mathbf{1}^{-/0/+}$.

	^{1}A($\mathbf{1}^-$;C_2)	^{2}A($\mathbf{1}$;C_2)	^{2}B($\mathbf{1}$;C_2)	$^2\mathbf{1}$(bs)[a]	$^2\mathbf{1}$(C_1)[b]	^{3}B($\mathbf{1}^+$;C_2)
E_{rel}	0.00	+57.02	+57.52	+56.67	+52.89	+176.72
$<S^2>$	0.000	0.753	0.752	0.750	0.750	2.001
ρ Mn2/Mn1	0.000	0.569	0.599	0.957/0.015	0.989/−0.003	1.025
ρ N2/N1	0.000	−0.031	0.032	−0.029/0.012	−0.019/0.019	−0.013
q Mn2/Mn1	+0.969	+0.990	+0.993	+1.010/+0.972	+1.023/+0.963	+1.022
q L[c]	−0.718	−0.520	−0.570	−0.537	−0.538	−0.398
q Cp2/Cp1	−0.501	−0.296	−0.288	−0.195/−0.390	−0.221/−0.374	−0.088
q CO(20)/CO(10)	−0.301	−0.207	−0.196	−0.114/−0.292	−0.102/−0.299	−0.100
q CO(21)/CO(11)	−0.308	−0.227	−0.224	−0.128/−0.326	−0.114/−0.338	−0.135

[a] Values from broken symmetry solution. [b] Values for the structure optimized without symmetry constraints. [c] L = bridging pyrazolate.

is not an energy consuming process: $^2\mathbf{1}$(bs) is only by 0.35 kcal mol^{-1} more stable than ^{2}A($\mathbf{1}$;C_2). In $^2\mathbf{1}$(bs), the spin is almost perfectly localized on Mn2 (ρMn2 = 0.975, ρMn1 = 0.015), in excellent agreement with the temperature-dependent EPR results for **1** in solution. Although the positive charges at Mn2 and Mn1 in $^2\mathbf{1}$(bs) do not differ much, taking into account the above-mentioned reorganization of electron density as well as comparing the data from Table 2 leads to the conclusion that not only the spin but also the charge is localized at the Mn2 center: close inspection reveals that the charge of the Mn2 atom in $^2\mathbf{1}$(bs) (+1.010) is nearly the same as in the $Mn^{II}Mn^{II}$ compound $\mathbf{1}^+$ (+1.022), while that of Mn1 (+0.972) is almost identical to the charge in the $Mn^{I}Mn^{I}$ complex $\mathbf{1}^-$ (+0.969). Thus, both the charge and spin distributions from the broken symmetry solution support a localized $Mn^{I}Mn^{II}$ ground state electronic structure of complex **1**. The same is valid for the optimized structure $^2\mathbf{1}(C_1)$ (calculated without symmetry constraints) which is 3.78 kcal mol^{-1} more stable than the broken symmetry solution $^2\mathbf{1}$(bs).

These results from DFT calculations are fully in line with the experimental IR and EPR spectroscopic findings discussed above. In accordance with the lack of any ^{55}Mn–^{14}N hyperfine coupling in the EPR experiments, the spin density on the pyrazolate-N atom is found to be negligible (Table 2). Finally, the calculated gas-phase CO stretching frequencies for geometry-optimized C_2-symmetric (isovalent) $\mathbf{1}^-$ and $\mathbf{1}^+$ reproduce well the experimental IR observations in solution, not only with respect to energies, but also with respect to band intensities (compare Table 3 and Figure 7). This once more corroborates our interpretation that the additional (low intensity) features in the IR spectra of $\mathbf{1}^-$ and $\mathbf{1}^+$ (Figure 7) arise from vibrational coupling of the adjacent metal dicarbonyl fragments. Likewise, the frequencies and band intensities calculated for mixed-valent $\mathbf{1}(C_1)$ are in excellent agreement with experimental findings. Interestingly, the calculated IR spectrum for the ^{2}A ground state of $\mathbf{1}(C_2)$ does not agree with the experimental findings.

Table 3. Frequencies [cm^{-1}] for the CO stretches of $\mathbf{1}^-$, **1** and $\mathbf{1}^+$ obtained experimentally, and calculated frequencies (B3LYP/6–311G*) (a scaling factor of 0.95 was applied); relative intensities are given in parentheses.

Symmetry[a]	$\mathbf{1}^-$ (exp)	$\mathbf{1}^-$ (calcd, C_2)	**1** (exp)	**1** (calcd, C_1)	$\mathbf{1}^+$ (exp)	$\mathbf{1}^+$ (calcd, C_2)
A	1816	1849 (0.09)	1843	1862 (0.94)	1941	1977 (0.19)
B	1848	1875 (1.00)	1912	1915 (0.67)	1964	1992 (1.00)
B	1896	1903 (0.38)	1958	1987 (1.00)	2021	2022 (0.73)
A	1919	1926 (0.66)	2028	2027 (0.86)	2041	2040 (0.93)

[a] The notation only applies to $\mathbf{1}^-$ and $\mathbf{1}^+$, which were geometry optimized in C_2 symmetry.

To interpret the optical spectra of $\mathbf{1}^-$ and mixed-valent **1** and to rationalize the lack of any observable IT transition for **1** in solution, we have finally studied the vertical excitation energies for the 12 and 20 lowest excited states of $\mathbf{1}^-(C_2)$ and $\mathbf{1}(C_1)$, respectively, by using the time-dependent DFT method (TD-DFT). These excited states predict electronic transitions in the energy regions 18921–28752 cm^{-1} for $\mathbf{1}^-(C_2)$ and 6129–22676 cm^{-1} for $\mathbf{1}(C_1)$. The character of the particular electronic transitions is analyzed in terms of contributing orbital excitations. Comparison of experimental band maxima with calculated energies of transitions that possess significant oscillator strength substantiates the spectral assignment. However, the oscillator strengths should only be used rather qualitatively to distinguish between very weak transitions that may also occur in the relevant energy region. The calculated energies of the transitions together with the oscillator strengths and the percentages of leading one-electron excitations are collected in Table 4.

For $\mathbf{1}^-(C_2)$ only one transition is listed, that is from the ground state ^{1}A to the fifth excited state 3^1B. The oscillator strength of all other 11 transitions is either equal zero or lower than 0.0002. The calculated excitation energy to the 3^1B state of 24710 cm^{-1} is in excellent agreement with the experimantal band at 400 nm (25000 cm^{-1}). Although this absorption apparently has multiconfigurational character (compare Table 4), its assignment as a $Mn^I \rightarrow \pi^*$(pyrazolate) MLCT transition (vide supra) is basically correct.

For $\mathbf{1}(C_1)$ we have omitted from Table 4 all transitions with oscillator strength lower than 0.0005, with the exception of the NIR energy region below 13000 cm^{-1}, where overlapping transitions are discernible in the experimental solid state spectrum. The one-electron transitions from the doublet ground state $^2\mathbf{1}(C_1)$ were calculated whithin the UHF scheme and are labeled by their consecutive numbers. It is seen from Table 4 that most excited states that give rise to electronic transitions in the visible and near UV energy region (transitions to excited states 9, 13, 18, and 19) have strong multiconfigurational character. According to the TD-DFT results they can be characterized as mixed d–d/MLCT or d–d/LMCT transitions. The mixed nature of these transitions

Table 4. Comparison of TD-DFT calculated excitation energies with experimental absorption maxima and assignment of low-lying electronic transition of $\mathbf{1}^-$ and **1**.[a,b]

	Experimental energies [cm^{-1}]	Calculated energies [cm^{-1}] (oscillator strength)	Excited state	Contributing orbital excitations
$\mathbf{1}^-(C_2)$	25000	24710 (0.0011)	3^1B	20% 55b(3dMn) → 59a(3dMn, π^*_L, π^*_{CO}) 30% 57a(3dMn) → 57b(3dMn, π^*_L, π^*_{CO}) 6% 55b(3dMn) → 60a(π^*_L, π^*_{CO}, 3dMn)
$\mathbf{1}(C_1)$	6083	6129 (0.0003)	1	100% 111β(3dMn1) → 112β(3dMn2)
		8273 (0.0007)	2	70% 108β(3dMn2, π_L) → 112β(3dMn2) 12% 110β(3dMn1) → 112β(3dMn2)
	8703	9796 (0.0004)	3	80% 110β(3dMn1) → 112β(3dMn2) 11% 108β(3dMn2, π_L) → 112β(3dMn2)
		12870 (0.0008)	6	92% 109β(3dMn1) → 112β(3dMn2)
		18238 (0.0012)	9	37% 112α(3dMn1) → 113α(3dMn2) 16% 111β(3dMn1) → 119β(3dMn1, π^*_L) 9% 112α(3dMn1) → 119α(3dMn1, π^*_L)
		20517 (0.0005)	13	14% 111α(3dMn1) → 113α(3dMn2) 14% 111α(3dMn1) → 119α(3dMn1, π^*_L) 7% 109β(3dMn1) → 119β(3dMn1, π^*_L) 5% 111α(3dMn1) → 120α(π^*_L)
	21368	22237 (0.0011)	18	21% 105α(3dMn2) → 113α(3dMn2) 17% 108β(3dMn2) → 113β(3dMn2) 11% 109α(π_L) → 114α(3dMn2) 5% 104α(3dMn2) → 113α(3dMn2)
		22502 (0.0008)	19	30% 104α(3dMn2) → 113α(3dMn2) 17% 104β(3dMn2, π_L) → 113β(3dMn2) 16% 105β(π_L) → 113β(3dMn2) 15% 105α(3dMn2) → 113α (3dMn2)
		22676 (0.0017)	20	35% 112α(3dMn1) → 115α(π^*_{CO}) 6% 103β(π_L) → 112β(3dMn2) 5% 111β(3dMn1) → 113β(3dMn2)

[a] Energies in cm^{-1}. Calculated oscillator strengths are given in parentheses. Electronic transitions from the ground state ^1A of $\mathbf{1}^-(C_2)$ and $^2\mathbf{1}(C_1)$ are described by leading orbital excitations with contributions greater than 5%. [b] The excited states of **1** are labeled by the consecutive numbers according to increasing energies.

might in part be due to the character of the involved MOs, which is determined by the particular calculational method used here. It has been discussed in the literature[47] that with respect to multiconfigurational approaches such as CASSCF/CASPT2, the Kohn–Sham orbitals are generally more delocalized over the metal centers and ligands to compensate for the monodeterminantal nature, and as a result the transitions calculated by TD-DFT may be expanded over many states.[47] Nevertheless, the calculated electronic transition to the 3^1B excited stated of $\mathbf{1}^-$ (24710 cm^{-1})—which according to TD-DFT includes mixed d–d/MLCT character—is in excellent agreement with and only slightly lower than the experimental band maximum at 25000 cm^{-1}, as has been pointed out above.

In the case of mixed-valent **1**, five excited states (9, 13, 18, 19, and 20) predict transition energies close to the experimental value of 21368 cm^{-1} (Table 4). Two of the transitions (9 and 13) have mixed d–d/MLCT character, while the other three (18, 19, and 20) possess d–d/LMCT character.

Thus, no unequivocal assignment of the visible part in the absorption spectrum of **1** is possible based on the TD-DFT results. Unfortunately, the use of multiconfigurational approaches for the large system studied here is out of the present computational possibilities.

In contrast to the UV/Vis part, the lowest excited states of **1** (which are found in the NIR region) do not show any pronounced multiconfigurational character. In particular, the first excited state of **1** is purely monoconfigurational and the TD-DFT energy for the electronic transition (6129 cm^{-1}) reproduces almost exactly the energy of the NIR band observed in the optical spectrum of solid **1** (6083 cm^{-1}). The shapes of the Kohn–Sham MOs involved in the NIR transitions of **1** are shown in Figure 11.

From Figure 11 and Table 4 it is evident that the electronic transitions calculated at 6129 cm^{-1}, 9796 cm^{-1}, and 12870 cm^{-1} (transitions to excited states 1, 3, and 6) represent 3d electron transfer from Mn1 to Mn2, that is they are true intervalence transitions (IT) of the mixed valence $Mn^{II}Mn^{I}$ complex **1**. The transition at 12870 cm^{-1} cannot be clearly identified in the experimental spectrum, but its oscillator strength is apparently quite low and the value of 9796 cm^{-1} is only slightly higher in energy than the broad experimental absorption centered at 8703 cm^{-1}.

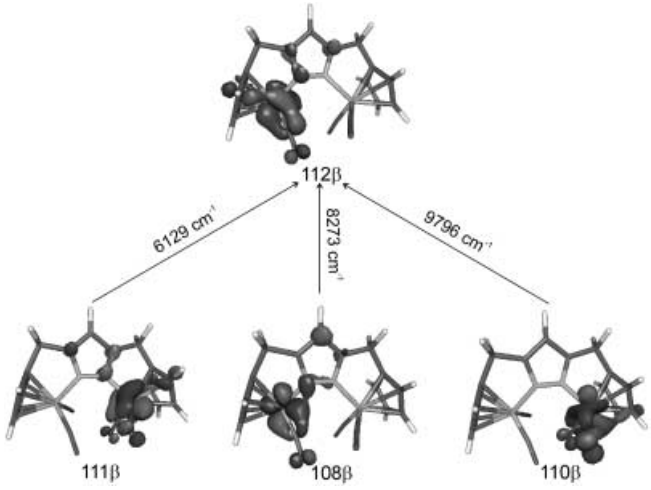

Figure 11. Shapes of the Kohn–Sham MOs involved in the lowest electronic transitions in **1**.

As has already been observed for 17-valence-electron $[CpMn(CO)_2L]$ complexes,[42] there is a low-energy NIR transition that has predominant ligand-field character. In the case of **1**, this transition (to excited state 2) is calculated to occur at 8273 cm^{-1}. It should be noted, however, that the 3d–3d electronic transition on Mn2 contributes only 70%, while

12% are again due to an IT process. Considering the general agreement between the calculated energies for the IT transitions and the experimental NIR absorptions observed for **1** in the solid state, it seems reasonable to assign the latter (in particular the lowest energy band at $\sim 6100\ cm^{-1}$) to IT processes. The absence of these IT absorptions in the solution optical spectra of **1** remains unexplained, but according to the TD-DFT calculations their oscillator strengths are apparently quite low, and hence the larger IT bandwidth expected for a class II system (according to the Hush theory, vide infra) as well as any further line-broadening effects may lead to their non-observability in solution.

Conclusion

Herein we report an in-depths analysis of the spectroscopic properties and electronic structure of an intriguing dimanganese complex in its $Mn^{I}Mn^{I}$ (**1**$^{-}$), mixed-valent $Mn^{I}Mn^{II}$ (**1**) and oxidized $Mn^{II}Mn^{II}$ (**1**$^{+}$) forms. Due to the rigid chelate arrangement of the suitably designed ligand scaffold, dissociation of the pyrazolate-bridged $CpMn(CO)_2$ subunits is prevented, and experimental findings indicate integrity of the bimetallic array in all three oxidation states. Strong electronic coupling in the mixed-valent complex has been corroborated by means of electrochemistry, variable-temperature EPR spectroscopy, IR spectroelectrochemistry, and UV/Vis/NIR spectroelectrochemistry, but time- (and temperature-)dependent valence detrapping is observed, which places **1** in class II according to the Robin and Day assignment, close to the class II/III transition. From variable-temperature EPR spectroscopy a rough estimate of the activation energy and the rate for thermal electron transfer can be deduced, with $E_{th}^{\ddagger} = 13.6\ kJ\,mol^{-1}$ and $k_{th} = 2.6 \times 10^{10}\ s^{-1}$ at 298 K. While the lack of any intervalence charge transfer (IT) transition for **1** in solution is quite unusual, the conclusions drawn from experiments are fully supported by DFT calculations that were carried out for all three forms of the dimanganese complex. A broken-symmetry treatment for mixed-valent **1** reveals almost perfect localization of both spin and charge on one Mn center, but only little energy gain with respect to the delocalized (C_2-symmetric) wave function. The structure of **1** that has been optimized without symmetry constraints, however, is $17.3\ kJ\,mol^{-1}$ more stable than the C_2-symmetric one. The highest occupied MOs are located at the Mn ions and are favorably arranged for π interactions with the bridging pyrazolate ligand. IR absorptions of **1**$^{-}$, **1**, and **1**$^{+}$ as well as the UV/Vis absorption of **1**$^{-}$ (which is mainly a MLCT transition) are well reproduced by the DFT and TD-DFT calculations, respectively. Most UV/Vis transitions of mixed-valent **1** have pronounced multiconfigurational character. The first excited state of **1**, however, is purely monoconfigurational and gives rise to an IT transitions in the NIR-energy region. The TD-DFT energies for the IT processes are in excellent agreement with the bands observed in the NIR region of the optical spectrum of solid **1**, but oscillator strengths for the IT transitions are calculated to be low, which in the presence of additional line-broadening effects might explain why these transitions are not observed in solution.

Experimental Section

General procedures and methods: All manipulations were carried out under an atmosphere of dry argon by employing standard Schlenk techniques. Complex **2** was prepared as reported in reference [20]. Solvents were dried according to established procedures, all other chemicals were used as purchased. Microanalyses: Mikroanalytische Laboratorien des Organisch-Chemischen Instituts der Universität Heidelberg. NMR spectra: Bruker AC 200 at 200.13 (^{1}H) and 50.32 (^{13}C) MHz; solvent signal as chemical shift reference ($CDCl_3$ $\delta_H = 7.27$, $\delta_C = 77.0$ ppm). Cyclic voltammetry: PAR equipment, (potentiostat/galvanostat 273), in 0.1 M NBu_4PF_6/CH_2Cl_2. Potentials in V on glassy carbon electrode, referenced to SCE at ambient temperature. IR spectra: Perkin-Elmer 983G; recorded as KBr pellets. FAB-MS spectra: Finnigan MAT 8230. UV/Vis spectra: Perkin-Elmer Lambda 19. EPR spectra: Bruker ELEXSYS E500, magnet B-E25. Spectroelectrochemistry: Self-constructed OTTLE cell comprising a Pt-mesh working and counter electrode and a silver wire as pseudeo-reference electrode sandwiched in between the CaF_2 windows of a conventional liquid IR cell. The working electrode is positioned in the center of the spectrometer beam with all other parts of the cell made non-transparent to the incident beam by means of an absorbing tape.[48]

Compound 3: $[CpMn(CO)_3]$ (2.50 g, 12.20 mmol) was dissolved in THF (50 mL), and *n*BuLi (4.80 mL of a 2.5 M solution in hexane) was added at $-78\,^{\circ}C$ by means of a syringe. After the mixture had been stirred for 1 h at low temperature, $ZnCl_2$ (1.70 g, 12.20 mmol) in THF (20 mL) was added and stirring was continued for 1 h. In a separate flask, a solution of the Pd^0 catalyst $[Pd(PPh_3)_2]$ was prepared by reducing a suspension of $[PdCl_2(PPh_3)_2]$ (0.14 g, 0.20 mmol) in THF (10 mL) with diisobutylaluminum hydride (DIBAH; 0.40 mL of a 1.0 M solution in hexane). This catalyst solution was transferred to the reaction mixture by using a canula, and a solution of 3,5-bis(bromomethyl)-1-tetrahydropyran-2-yl pyrazole (**2**; 1.70 g, 5 mmol) in THF (20 mL) was then added. Stirring was continued for 1 h at $-78\,^{\circ}C$ and finally for 72 h at room temperature under exclusion of light. The reaction mixture was hydrolyzed with brine, and the organic phase separated and dried with $MgSO_4$. After evaporation of all volatile material under reduced pressure, the crude product was purified by column chromatography (silica, CH_2Cl_2/light petroleum 1:1, R_f (Et_2O/light petroleum) = 0.33). The product **3** was obtained as a light brown oil (1.30 g, 2.22 mmol, 44%). ^{1}H NMR ($CDCl_3$): $\delta = 1.67-1.72$ (br, kb, 3H; $CH_2^{thp,4/5}$), 1,96–2.14 (br, kb, 2H; $CH_2^{thp,3/4}$), 2.45 (br, m, 1H; $CH_2^{thp,3}$), 3.59 (br, d, $^3J = 4.0$ Hz, 1H; $CH_2^{thp,6}$), 3.69 (br, s, 4H; CH_2), 4.08 (br, d, $^3J = 10.8$ Hz, 1H; $CH_2^{thp,6}$), 4.63–4.75 (br, kb, 8H; CH^{Cp}), 5.25–5.33 (br, m, 1H; $CH_2^{thp,2}$), 5.97 ppm (br, s, 1H; CH^{pz}); ^{13}C NMR ($CDCl_3$): $\delta = 22.4$ ($CH_2^{thp,4}$), 24.1, 24.6 (CH_2), 26.9 ($CH_2^{thp,5}$), 29.3 ($CH_2^{thp,3}$), 67.5 ($CH_2^{thp,6}$), 80.9, 81.3, 81.5, 81.7, 83.1, 83.5 (CH^{Cp}), 84.5 ($CH_2^{thp,2}$) 105.6 (CH^{pz}), 141.5, 149.4 (C), 224.6 ppm (CO); IR (film): $\tilde{\nu} = 3103$ w, 2936 m, 2849 m, 2011 vs, 1911 vs, 1546 m, 1462 m, 1427 m, 1259 m, 1203 m, 1081 s, 1058 m, 1040 s, 1003 m, 918 w, 846 m, 667 s, 634 vs cm^{-1}; MS (FAB, nibeol): *m/z* (%): 585 (5) [$M^+ + H^+$], 556 (5) [$M^+ - CO$], 500 (100) [$M^+ - DHP$], 416 (40) [$M^+ - 3\,CO - DHP$]; elemental analysis calcd (%) for $C_{26}H_{22}Mn_2N_2O_7$ (584.34): C 53.44, H 3.79, N 4.79; found: C 53.92, H 4.08, N 5.02.

Compound 4: Compound **3** (1.30 g, 2.22 mmol) was dissolved in ethanol (50 mL), and a saturated solution of HCl in ethanol (10 mL) was added. After the mixture had been stirred overnight, the volume of the reaction mixture was reduced to about 10 mL under reduced pressure and diethyl ether (50 mL) was added to precipitate the hydrochloride salt **2**·HCl. This was separated by filtration and treated with aqueous ammonia and CH_2Cl_2 (50 mL). The organic phase was dried with $MgSO_4$ and the solvent evaporated under vacuum. Diffusion of light petroleum into a solution of the product in a small amount of CH_2Cl_2 gave light yellow crystals of compound **4** (0.73 g, 1.46 mmol, 66%). ^{1}H NMR ($CDCl_3$, 233 K): $\delta = 3.55$ (br, s, 4H; CH_2), 4.63 (br, s, 8H; CH^{Cp}), 6.01 ppm (br, s, 1H; CH^{pz}); ^{13}C NMR (CD_2Cl_2, 233 K): $\delta = 25.1$, 27.7 (CH_2), 83.3 (CH^{Cp}), 104.0 (CH^{pz}), 141.9, 151.4 (C), 225.9 ppm (CO); IR (KBr): $\tilde{\nu} = 2632$ w, 2025 vs, 2005 vs, 1999 vs, 1965 vs, 1910 vs, 1597 w, 1258 w, 1161 w, 1030 w, 845 w, 663 m, 663 m cm^{-1}; UV/Vis (THF): λ (ε) = 326 (2477); MS (EI): *m/z* (%): 499.9 (100) [M^+], 416 (90) [$M^+ - 3\,CO$]; elemental analysis calcd (%) for $C_{21}H_{14}Mn_2N_2O_6$ (500.22): C 50.42, H 2.82, N 5.60; found: C 50.29, H 2.93, N 5.64.

Compound K$^+$1$^-$: A solution of **4** (0.29 g, 0.58 mmol) in THF (200 mL) was irradiated by means of a high-pressure mercury lamp in a quartz apparatus

for 15 min at −40 °C, which caused the reaction mixture to turn deep red. The progress of the reaction was monitored by IR spectroscopy in the CO stretching region (2015, 1927 before irradiation; 1916, 1843 after irradiation). After the mixture had been warmed to room temperature, KO*t*Bu (0.65 g, 0.58 mmol) was added and the reaction mixture was left stirring for 1 h. All volatile material was then removed under vacuum and the red residue was washed with light petroleum and dissolved in a small amount of THF. Slow diffusion of light petroleum into the solution deposited red crystals of $K^+\mathbf{1}^- \cdot 0.9\,THF$ (yield: 0.18 g, 0.37 mmol, 63.7 %). IR (KBr): $\tilde{\nu}$ = 1911 vs, 1885 m, 1844 vs cm^{-1}; IR (THF): $\tilde{\nu}$ = 1916 vs, 1891 m, 1849 vs cm^{-1}; UV/Vis (THF): $\lambda_{max}(\varepsilon)$ = 400 nm (460); MS (FAB) m/z (%): 482 (10) [M^+], 443 (20) [$M^+ - K$], 387 (45) [$M^+ - K - 2CO$], 345; elemental analysis calcd (%) for $C_{19}H_{13}KMn_2N_2O_4$ (482.29): C 49.82, H 3.81, N 5.05; found: C 49.24, H 3.81, N 5.04.

Compound 1: A solution of **4** (0.22 g, 0.43 mmol) was irradiated as described above. After the mixture had been warmed to room temperature, KO*t*Bu (0.05 g, 0.43 mmol) was added and the reaction mixture stirred for 1 h. All volatile material was evaporated under reduced pressure and the residue washed with light petroleum and then taken up in THF (50 mL). $AgBF_4$ (0.08 g, 0.40 mmol) was added in one portion. After 1 h, all solid material was filtered off and the solvent was removed under vacuum. The remaining red solid was redissolved in CH_2Cl_2 and filtered again to remove any KBF_4. Finally, the solvent was evaporated to yield the product **1**. IR (KBr): $\tilde{\nu}$ = 2025 s, 1954 vs, 1896 s, 1821 vs cm^{-1}; IR (THF): $\tilde{\nu}$ = 2027 vs, 1952 vs, 1899 s, 1827 vs cm^{-1}; UV/Vis (THF): $\lambda_{max}(\varepsilon)$: 288 (7298), 412 (1864), 468 nm (2236).

Calculation details: The DFT calculations were carried out with the B3LYP method[49] by using a single extended all-electron basis set. For Mn we chose Wachters (14s, 9p, 5d) basis[50] augmented with one 4f polarization function. The standard 6–311G* basis was used for the remaining atoms.[51] The doublet and triplet states were calculated with the UHF procedure. Geometry optimization was carried out by using analytical gradient procedures. The presented structures correspond to fully converged geometries with gradients and displacements below the thresholds implemented in Gaussian 98. Vibrational frequencies were obtained from analytic calculation of the Hessian matrices. The calculated frequencies were scaled by a factor 0.95. Vertical excitation energies were studied by using the TD-DFT method with the same functionals and basis sets as described above. The calculations have been carried out with the Gaussian 98 program.[52] For graphical displays we have used the MOLEK 9000[53] and MOLDEN[54] programs.

X-ray crystallography: Crystal structure of **4** ($C_{21}H_{14}Mn_2N_2O_6$, M_r = 500.2): triclinic, $P\bar{1}$, a = 7.537(2), b = 11.919(2), c = 12.383(3) Å, α = 72.59(3), β = 72.49(3), γ = 82.75(3), V = 1012(2) $Å^3$, Z = 2, ρ_{calcd} = 1.642 $g\,cm^{-3}$, $\mu(Mo_{K\alpha})$ = 1.29 mm^{-1}, $2\theta_{max}$ = 55.0°, 4574 independent reflections (R_{int} = 0.023), 3583 observed [$I > 2\sigma(I)$], 336 parameters; final *R1* [$I > 2\sigma(I)$] = 0.036, *wR2* (all data) = 0.087, goodness of fit on F^2 = 1.028, largest difference peak +0.31/−0.52 $e\,Å^{-3}$. Crystal structure of $[K^+\mathbf{1}^-]_4 \cdot 3.6\,THF$ ($C_{76}H_{52}K_4Mn_8N_8O_{16} \cdot 3.6\,THF$, M_r = 2188.8): monoclinic, $P2_1/c$, a = 23.071(5), b = 25.404(5), c = 15.501(3) Å, β = 91.14(3), V = 9083(3) $Å^3$, Z = 4, ρ_{calcd} = 1.601 $g\,cm^{-3}$, $\mu(Mo_{K\alpha})$ = 1.33 mm^{-1}, $2\theta_{max}$ = 55.0°, 20751 independent reflections (R_{int} = 0.093), 12009 observed [$I > 2\sigma(I)$], 1192 parameters; final *R1*[$I > 2\sigma(I)$] = 0.076, *wR2* (all data) = 0.127, goodness of fit on F^2 = 1.020, largest difference peak +0.73/−0.48 $e\,Å^{-3}$. Data were collected on a Nonius Kappa CCD diffractometer at 200 K by using $Mo_{K\alpha}$ radiation (λ = 0.71073 Å). Non-hydrogen atoms were refined in anisotropic models. Hydrogen atoms were placed at calculated positions and allowed to ride on the atoms they are attached to. The structure was solved by direct methods with the SHELXS-97 and refined with the SHELXL-97 programs.[55] CCDC-162376 (**4**) and CCDC-162374 ($[K^+\mathbf{1}^-]_4$) contain the supplementary crystallographic data for this paper. These data can be obtained free of charge via www.ccdc.cam.ac.uk/conts/retrieving.html (or from the Cambridge Crystallographic Data Centre, 12 Union Road, Cambridge CB2 1EZ, UK; fax: (+44) 1223-336-033; or deposit@ccdc.cam. uk).

Acknowledgement

F.M. sincerely thanks Prof. Dr. G. Huttner for his generous support. We are grateful to Prof. Dr. G. Huttner and Prof. Dr. W. Kaim for allowing the use of facilities in Heidelberg and Stuttgart. Funding by the DFG (SFB 247, Graduiertenkollegs-Stipendium to J.C.R.), the Fonds der Chemischen Industrie (F.M.) and the VW-Stiftung (R.F.W.) is acknowledged. I. H.-K. thanks the University of Münster, the SFB 424 and especially Prof. Dr. G. Erker and Prof. Dr. S. Grimme for the possibilty to continue scientific research.

[1] a) G. Süss-Fink, *Angew. Chem.* **1994**, *106*, 71–73; *Angew. Chem. Int. Ed. Engl.* **1994**, *33*, 67–69; b) M. W. Göbel, *Angew. Chem.* **1994**, *106*, 1201–1203; *Angew. Chem. Int. Ed. Engl.* **1994**, *33*, 1141–1143; c) L. Que, Jr., Y. Dong, *Acc. Chem. Res.* **1996**, *29*, 190–196; d) H. Steinhagen, G. Helmchen, *Angew. Chem.* **1996**, *108*, 2489–2492; *Angew. Chem. Int. Ed. Engl.* **1996**, *35*, 2339–2342; e) E. K. van den Beuken, B. L. Feringa, *Tetrahedron* **1998**, *54*, 12985–13011.

[2] a) S. R. Collinson, D. E. Fenton, *Coord. Chem. Rev.* **1996**, *148*, 19–40; b) H. Okawa, H. Sakiyama, *Pure Appl. Chem.* **1995**, *67*, 273–280; b) D. E. Fenton, H. Okawa, *Chem. Ber.* **1997**, *130*, 433–442; c) D. G. McCollum, B. Bosnich, *Inorg. Chim. Acta* **1998**, *270*, 13–19; d) M. Shibasaki, H. Sasai, T. Arai, T. Iida, *Pure Appl. Chem.* **1998**, *70*, 1027–1034.

[3] a) O. Kahn, *Angew. Chem.* **1985**, *97*, 837–853; *Angew. Chem. Int. Ed. Engl.* **1985**, *24*, 834–850; b) O. Kahn, *Adv. Inorg. Chem.* **1995**, *43*, 179–259.

[4] a) M. B. Robin, P. Day, *Adv. Inorg. Chem. Radiochem.* **1967**, *10*, 247–422; N. S. Hush, *Coord. Chem. Rev.* **1985**, *64*, 135; c) R. A. Marcus, *Pure Appl. Chem.* **1997**, *69*, 13–29.

[5] a) M. D. Ward, *Chem. Soc. Rev.* **1995**, *24*, 121–134; b) H. Vahrenkamp, A. Geiss, G. N. Richardson, *J. Chem. Soc. Dalton Trans.* **1997**, *20*, 3643–3651.

[6] a) C. Creutz, *Prog. Inorg. Chem.* **1983**, *30*, 1–73; b) R. C. Crutchley, *Adv. Inorg. Chem.* **1994**, *41*, 273–325.

[7] K. G. Caulton, *Coord. Chem. Rev.* **1981**, *38*, 1–43.

[8] W. Kaim, R. Gross, *Comments Inorg. Chem.* **1988**, *7*, 269–285.

[9] See for example: a) T. Würminghausen, D. Sellmann, *J. Organomet. Chem.* **1980**, *199*, 77–85; b) W. Gäde, E. Weiss, *J. Organomet. Chem.* **1981**, *222*, 451–460; c) D. Sellmann, J. Müller, P. Hofmann, *Angew. Chem.* **1982**, *94*, 708–709; *Angew. Chem. Int. Ed. Engl.* **1982**, *21*, 691; d) A. Winter, G. Huttner, L. Zsolnai, P. Kroneck, M. Gottlieb, *Angew. Chem.* **1984**, *96*, 986–987; *Angew. Chem. Int. Ed. Engl.* **1984**, *23*, 975; e) R. Gross, W. Kaim, *Angew. Chem.* **1985**, *97*, 869–870; *Angew. Chem. Int. Ed. Engl.* **1985**, *24*, 856–858; f) W. A. Herrmann, H.-J. Kneuper, E. Herdtweck, *Angew. Chem.* **1985**, *97*, 1060–1061; *Angew. Chem. Int. Ed. Engl.* **1985**, *24*, 1062–1063; g) D. Sellmann, J. Müller, *J. Organomet. Chem.* **1985**, *281*, 249–262; h) A. Winter, G. Huttner, M. Gottlieb, I. Jibril, *J. Organomet. Chem.* **1985**, *286*, 317–327; i) G. Huttner, K. Evertz, *Acc. Chem. Res.* **1986**, *19*, 406–413; j) R. Gross, W. Kaim, *Inorg. Chem.* **1987**, *26*, 3596–3600; k) W. A. Herrmann, H.-J. Kneuper, E. Herdtweck, *Chem. Ber.* **1989**, *122*, 437–444; l) G. Huttner, F. Ettel, L. Zsolnai, *Angew. Chem.* **1989**, *101*, 1525–1527; *Angew. Chem. Int. Ed. Engl.* **1989**, *28*, 1496–1498; m) H. Braunwarth, P. Lau, G. Huttner, M. Minelli, D. Günauer, L. Zsolnai, I. Jibril, K. Evertz, *J. Organomet. Chem.* **1991**, *411*, 383–394; n) P. Lau, H. Braunwarth, G. Huttner, D. Günauer, K. Evertz, W. Imhof, C. Emmerich, L. Zsolnai, *Organometallics* **1991**, *10*, 3861–3873.

[10] a) R. Gross, W. Kaim, *Angew. Chem.* **1984**, *96*, 610–611; b) R. Groß, W. Kaim, *Inorg. Chem.* **1986**, *25*, 498–506; c) R. Gross-Lannert, W. Kaim, B. Olbrich-Deussner, *Inorg. Chem.* **1990**, *29*, 5046–5053.

[11] R. Gross, W. Kaim, *Inorg. Chem.* **1986**, *25*, 4865–4870.

[12] a) C. G. Atwood, W. E. Geiger, *J. Am. Chem. Soc.* **1993**, *115*, 5310–5311; b) C. G. Atwood, W. E. Geiger, T. E. Bitterwolf, *J. Electroanal. Chem.* **1995**, *397*, 279–285.

[13] C. A. Atwood, W. E. Geiger, *J. Am. Chem. Soc.* **2000**, *122*, 5477–5485.

[14] J. C. Röder, F. Meyer, E. Kaifer, *Angew. Chem.* **2002**, *114*, 2414–2417; *Angew. Chem. Int. Ed.* **2002**, *41*, 2304–2306.

[15] a) J. Okuda, *Comments Inorg. Chem.* **1994**, *16*, 185–205; b) P. Jutzi, U. Siemeling, *J. Organomet. Chem.* **1995**, *500*, 175–185; c) P. Jutzi, Dahlhaus, J. *Coord. Chem. Rev.* **1994**, *137*, 179–199; d) C. Müller, D. Vos, P. Jutzi, *J. Organomet. Chem.* **2000**, *600*, 127–143.

[16] J. C. Röder, F. Meyer, H. Pritzkow, *Organometallics* **2001**, *20*, 811–817.

[17] See for example: a) F. Meyer, P. Rutsch, *Chem. Commun.* **1998**, 1037 – 1038; b) F. Meyer, E. Kaifer, P. Kircher, K. Heinze, H. Pritzkow, *Chem. Eur. J.* **1999**, *5*, 1617 – 1630; c) J. Ackermann, F. Meyer, E. Kaifer, H. Pritzkow, *Chem. Eur. J.* **2002**, *8*, 247 – 258.

[18] a) M. E. Huttenloch, J. Diebold, U. Rief, H. H. Brintzinger, *Organometallics* **1992**, *11*, 3600 – 3607; b) M. Enders, G. Kohl, H. Pritzkow, *J. Organomet. Chem.* **2001**, *622*, 66 – 73.

[19] J. C. Röder, F. Meyer, R. F. Winter, E. Kaifer, *J. Organomet. Chem.* **2002**, *641*, 113 – 120.

[20] J. C. Röder, F. Meyer, M. Konrad, S. Sandhöfner, E. Kaifer, H. Pritzkow, *Eur. J. Org. Chem.* **2001**, 4479 – 4487.

[21] J. C. Röder, F. Meyer, E. Kaifer, unpublished results.

[22] Z. Pang, T. J. Burkey, *Organometallics* **1997**, *16*, 120 – 123.

[23] For Ru: J. R. Perera, M. J. Heeg, H. B. Schlegel, C. W. Winter, *J. Am. Chem. Soc.* **1999**, *121*, 4536 – 4537; for K: Z. Hu, S. M. Gorun, *Inorg. Chem.* **2001**, *40*, 667 – 671; for Tl: G. B. Deacon, E. E. Delbridge, C. M. Forsyth, B. W. Skelton, A. H. White, *J. Chem. Soc. Dalton Trans.* **2000**, 745 – 751; for Eu: G. B. Deacon, A. Gitlits, P. W. Roesky, M. R. Bürgstein, K. C. Lim, B. W. Skelton, A. H. White, *Chem. Eur. J.* **2001**, *7*, 127 – 138; for Ba: A. Steiner, G. T. Lawson, B. Walfort, D. Leusser, D. Stalke, *J. Chem. Soc. Dalton Trans.* **2001**, 219 – 221.

[24] J. E. Cosgriff, G. B. Deacon, *Angew. Chem.* **1998**, *110*, 298 – 299; *Angew. Chem. Int. Ed.* **1998**, *37*, 286 – 287.

[25] $d(\mathrm{K1}\cdots\mathrm{C/O}) = 3.195/3.023$ Å has been observed in $K_3[Mn_3(CO_{12})]$: W. Schatz, H.-P. Neumann, B. Nuber, B. Kanellakopulos, M. L. Ziegler, *Chem. Ber.* **1991**, *124*, 453 – 463.

[26] F. H. Allen, Davis, J. E., J. J. Galloy, O. Johnson, O. Kennard, C. F. Macrae, E. M. Mitchell, G. F. Mitchell, J. M. Smith, D. G. Watson, *J. Chem. Inf. Comput. Sci.* **1991**, *31*, 187.

[27] Values versus the saturated calomel electrode (SCE). i_{pa}/i_{pc} close to 1; $i_{pc}/v^{1/2} \approx$ const.

[28] D. Astruc, *Electron Transfer and Radical Processes in Transition-Metal Chemistry*, Wiley-VCH, New York, **1995**.

[29] Departures from first-order line spacings result from coincidence of the x and z principal axes of the g and ^{55}Mn hyperfine tensors: R. D. Pike, A. L. Rieger, P. H. Rieger, *J. Chem. Soc. Faraday Trans.* **1989**, *85*, 3913 – 3925.

[30] R. R. Gagné, C. A. Koval, T. J. Smith, M. C. Cimlino, *J. Am. Chem. Soc.* **1979**, *101*, 4571 – 4580; all symbols have their usual meanings. k_{th} is taken to be equal to the EPR liftime at the coalescence temperature ($5.5 \cdot 10^8$ s^{-1}). E^*_{th} is supposed to not change in the given temperature range and adiabatic electron transfer is assumed. See also: a) R. C. Long, D. N. Hendrickson, *J. Am. Chem. Soc.* **1983**, *105*, 1513 – 1521; b) S. K. Dutta, S. B. Kumar, S. Bhattacharyya, E. R. T. Tiekink, M. Chaudhury, *Inorg. Chem.* **1997**, *36*, 4954 – 4960.

[31] R. Kirmse, J. Stach, *ESR-Spektroskopie*, Akademie-Verlag, Berlin, **1985**.

[32] A. Davison, M. L. H. Green, G. Wilkinson, *J. Chem. Soc.* **1961**, 3172 – 3177.

[33] N. G. Connelly, Z. Demidowicz, R. L. Kelly, *J. Chem. Soc. Dalton Trans.* **1975**, 2335 – 2340.

[34] The absorption of IR radiation occurs roughly on the time scale of a vibrational period (i.e. $1/\tilde{\nu}$), which for $\tilde{\nu}(\mathrm{CO}) = 2000$ cm^{-1} is 17 fs (1.7×10^{-14} s).

[35] $E_{1/2}$ for **5** is a little lower than the mean value for $\mathbf{1}^{-/0}$ and $\mathbf{1}^{0/+}$, but it should be noted that for solubility reasons different solvents have been used in the cyclovoltammetric experiments (CH_2Cl_2 in the case of **5**, THF in the case of **1**).

[36] M. E. Stoll, S. R. Lovelace, W. E. Geiger, H. Schimanke, I. Hyla-Kryspin, R. Gleiter, *J. Am. Chem. Soc.* **1999**, *121*, 9343 – 9351.

[37] Systems in the class II-III transition are defined by the rate constant for adiabatic intramolecular electron transfer being intermediate between the solvent reorganisation frequency ($10^{11} - 10^{12}$ s^{-1}) and typical bond vibration frequencies ($10^{13} - 10^{14}$ s^{-1}), that is, solvent modes are averaged but inner-shell modes are not.[38]

[38] a) D. D. Konstantinos, C. M. Hartshorn, T. J. Meyer, *Chem. Rev.* **2001**, *101*, 2655 – 2685; b) B. S. Brunschwig, C. Creutz, N. Sutin, *Chem. Soc. Rev.* **2002**, *31*, 168 – 184.

[39] P. J. Giordano, M. S. Wrighton, *Inorg. Chem.* **1977**, *16*, 160 – 166.

[40] a) J. Poppe, M. Moscherosch, W. Kaim, *Inorg. Chem.* **1993**, *32*, 2640 – 2643; b) W. Kaim, W. Bruns, S. Kohlmann, M. Krejcik, *Inorg. Chim. Acta* **1995**, *229*, 143 – 151.

[41] a) D. N. Hendrickson, S. M. Oh, T.-Y. Dong, T. Kambara, M. J. Cohn, M. F. Moore, *Comments Inorg. Chem.* **1985**, *4*, 329 – 349; P. Chen, T. J. Meyer, *Chem. Rev.* **1998**, *98*, 1439 – 1477.

[42] C. G. Atwood, W. E. Geiger, *J. Am. Chem. Soc.* **1984**, *106*, 10849 – 10850.

[43] a) E. M. Kober, N. A. Goldsby, D. N. S. Narayan, T. J. Meyer, *J. Am. Chem. Soc.* **1983**, *105*, 4303 – 4309; b) R. H. Magnuson, P. A. Lay, H. Taube, *J. Am. Chem. Soc.* **1983**, *105*, 2507 – 2509; c) U. Sinha, M. D. Lowery, W. S. Hammack, D. N. Hendrickson, H. G. Drickamer, *J. Am. Chem. Soc.* **1987**, *109*, 7340 – 7345; d) A. J. Roberts, J. T. Hupp, *Inorg. Chem.* **1992**, *31*, 157 – 160.

[44] a) J. W. Hershberger, R. J. Klingler, J. K. Kochi, *J. Am. Chem. Soc.* **1983**, *105*, 61 – 73; b) P. M. Zizelman, C. Amatore, J. K. Kochi, *J. Am. Chem. Soc.* **1984**, *106*, 3771 – 3784.

[45] a) L. S. Cederbaum, W. Domcke, *Chem. Phys.* **1977**, *25*, 189 – 196; b) W. H. E. Schwarz, T. C. Chang, U. Seeger, K. H. Hwang, *Chem. Phys.* **1987**, *117*, 73 – 89.

[46] I. Hyla-Kryspin. R. Gleiter, G. E. Herberich, M. Benard, *Organometallics* **1994**, *13*, 1975 – 1805, and references therein.

[47] M. Turki, Ch. Daniel, S. Záliš, A. Vlèek, Jr., J. van Slagern, D. J. Stufkens, *J. Am. Chem. Soc.* **2001**, *123*, 11431 – 11440.

[48] M. Kreijcik, M. Daniek, F. Hartl, *J. Electroanal. Chem.* **1991**, *317*, 179.

[49] a) A. D. Becke, *J. Chem. Phys.* **1993**, *98*, 5648 – 5652; b) S. H. Vosko, L. Wilk, M. Nusair, *Can. J. Phys.* **1980**, *58*, 1200 – 1211; c) C. Lee, W. Yang, R. G. Parr, *Phys. Rev. B* **1988**, *37*, 785 – 789.

[50] A. J. H. Wachters, *J. Chem. Phys.* **1970**, *52*, 1033 – 1036.

[51] R. Krishnan, J. S. Binkley, R. Seeger, J. A. Pople, *J. Chem. Phys.* **1980**, *72*, 650 – 654.

[52] Gaussian 98 (Revision A.7), M. J. Frisch, G. W. Trucks, H. B. Schlegel, G. E. Scuseria, M. A. Robb, J. R. Cheeseman, V. G. Zakrzewski, J. A. Montgomery, R. E. Stratmann, J. C. Burant, S. Dapprich, J. M. Millam, A. D. Daniels, K. N. Kudin, M. C. Strain, O. Farkas, J. Tomasi, V. Barone, M. Cossi, R. Cammi, B. Mennucci, C. Pomelli, C. Adamo, S. Clifford, J. Ochterski, G. A. Petersson, P. Y. Ayala, Q. Cui, K. Morokuma, D. K. Malick, A. D. Rabuck, K. Raghavachari, J. B. Foresman, J. Cioslowski, J. V. Ortiz, B. B. Stefanov, G. Liu, A. Liashenko, P. Piskorz, I. Komaromi, R. Gomperts, R. L. Martin, D. J. Fox, T. Keith, M. A. Al-Laham, C. Y. Peng, A. Nanayakkara, C. Gonzalez, M. Challacombe, P. M. W. Gill, B. G. Johnson, W. Chen, M. W. Wong, J. L. Andres, M. Head-Gordon, E. S. Replogle, J. A. Pople, Gaussian, Inc., Pittsburgh, PA, **1998**.

[53] P. Bischof, *Molek*-9000, Universität Heidelberg, **2000**.

[54] G. Schaftenaar, J. H. Noordik, Molden: a pre- and post-processing program for molecular and electronic structures, *J. Comput.-Aided Mol. Des.* **2000**, *14*, 123 – 134.

[55] a) G. M. Sheldrick, SHELXL-97, Program for Crystal Structure Refinement, University of Göttingen, Göttingen (Germany), **1997**; b) G. M. Sheldrick, SHELXS-97, Program for the Solution of Crystal Structures, University of Göttingen, Göttingen (Germany), **1997**.

Received: November 25, 2002 [F4606]